Supporting Information

The Gradual Introduction of Multiple Active Sites in Quest of High Activity Metal-Free Oxygen Reduction Catalysts and Exploring the Synergistic Effect

Qi Guo,[a] Shuai-Ma,[a] Qi-Long Wu,[b] Zhi-Zhuang Liu,[a] Zhao-Quan Yao,*[a] Shuai Li,[a] Jiong-Peng Zhao*[a] and Fu-Chen Liu*[a]

1. Experimental Section

1. Materials and instrumentation

Materials

All reagents were used without any further purification. Before calcining, the system was purged for 30 min with nitrogen gas to ensure the removal of oxygen from the furnace.

Characterization

Powder X-ray diffraction (XRD) data of the samples were measured by the Rigaku corporation Ultima IV. The morphologies structures of the samples were measured by using the Scanning electron microscope (ZEISS MERLIN Compact) and Transmission electron microscope (FEI Tecnai G2 F30). X-ray photoelectron spectroscopy (XPS) images were collected on a Thermo Scientific Escalab 250 Xi XPS spectrometer. Raman scattering spectra (HORIBA JOBIN YVON S.A.S. HORIBA EVOLUTION) were recorded with a laser excitation wavelength of 532 nm. N_2 sorption analysis were conducted by the Micromeritics ASAP 2020 at 77 K, and the surface area was calculated with Barrett-Emmett-Teller (BET).

Synthesis of ZnO@MAF-6 Precursor. In a typical synthesis, 3.84 g of $Zn(CH_3COO)_2 \cdot 2H_2O$ was added into 350 mL of ethanol at 75°C, the mixture refluxed for 20 minutes to completely dissolve, followed by adding 15 mL of KOH ethanol solution (2.2 $mol \cdot L^{-1}$) under refluxing. After refluxed for 20 min, added 50 mL $Zn(NO_3)_2 \cdot 6H_2O$ of ethanol solution (0.1 mol L^{-1}) under stirring conditions. Subsequently, collect the mixture with a centrifuge (9000 rpm, 1 min). Then 3.5 g of the above product was immersed into 100 mL of dimethylformamide (DMF) to form a homogeneous solution, and 2.1 g of 2-ethylimidazole were added into the above mixture and stirred about 24 h. After that, large amount of ZnO@MAF-6 sample was collected and washed once with ethanol and dried under vacuum at 40°C for 10 h.

Synthesis of MAF-6 Precursor. MAF-6 was synthesized according to a previously reported method.[1] 80 mL of $Zn(OH)_2$ (0.39 g) in 25% ammonia solution was added to 2-ethylimidazole (0.77 g) in the mixing of cyclohexane (16 mL) and methanol (60 mL). The mixture was then incubated for 24 h at room temperature with stirring. After that the MAF-6 powder was collected by centrifugation and finally dried under vacuum at 40°C 10 h.

Synthesis of N-DC (or N-C). N-DC was prepared from ZnO@MAF-6 and N-C was prepared from MAF-6. Typically, ZnO@MAF-6 (or MAF-6) was annealed at 1000°C for 2 h with a ramp rate of 10°C/min under a nitrogen atmosphere.

Synthesis of N/S-DC (or N/S-C). Transfer as-prepared N-DC (or N-C) to the downstream of the tube furnace with excess sulfur powder upstream was annealed at 400°C for 2 h with a ramp rate of 10°C/min under nitrogen atmosphere.

Synthesis of DC (or S-DC). Transfer N-DC (or N/S-DC) was annealed at 1100°C for 3 h with a ramp rate of 10°C/min under nitrogen atmosphere.

Electrochemical Measurements

All the electrochemical measurements were conducted on a CHI760E electrochemical workstation with a standard three-electrode system. Applying each of the catalyst inks onto a glassy carbon rotating disk electrode (RDE, diameter, 5 mm) or rotating ring-disk electrode (RRDE, disk diameter: 5.5 mm) was used as the working electrode, carbon rod was used as counter electrode, and an Ag/AgCl (3 M KCl) was used as reference electrode. To prepare the catalyst-coated working electrode, 6 mg of the as-synthesized catalyst was dispersed in the mixing solution of 500 μL H_2O, 500 μL EtOH and 50 μL nafion (5%) under sonication for 1 h to form a homogeneous catalyst ink. A 12 μL amount of the mixture was dropped onto a polished glassy carbon electrode (5 mm in diameter) in sequence and dried in air. All the recorded potential was converted to reversible hydrogen electrode (RHE) as follows:

$E_{RHE} = E_{Ag/AgCl} + E_{Ag/AgCl}^{\Theta} + 0.059\ pH$

ORR performances of as-prepared catalysts and commercial 20% Pt/C were measured in 0.1 M $HClO_4$ or 0.1 M KOH aqueous solution at room temperature. The electrochemistry measurements were represented with 95% iR compensation rate. linear sweep voltammetry (LSV) polarization curves and cyclic voltammetry (CV) were performed in Ar or O_2 saturated electrolyte. LSV polarization curves were measured with a sweep rate of 10 mV s^{-1} in rotating speed of 1600 rpm. LSV at different rotation rates were recorded in different rotating speed from 400 to 2500 rpm. CV was scanned at a scan rate of 50 mV s^{-1}. The tolerance to methanol test was carried out by *I-T* test at 0.50 V vs. RHE in a O_2-saturated solution along with the injection of methanol (1 M) at the time of 1500 second. Electrochemical stability was measured using *I-T* test at 0.5 V versus RHE at a rotation speed of 1600 rpm in O_2-saturated electrolyte.

The electron transfer number (n) and the hydrogen peroxide yield (%) were calculated from the RRDE measurement according to the following equation:

$$n = \frac{4I_d}{I_d + I_r / N} \quad (1)$$

$$H_2O_2(\%) = 200 \times \frac{I_r / N}{I_d + I_r / N} \quad (2)$$

where Id: disk current; Ir: ring current; N: ring collection efficiency (38.6%).

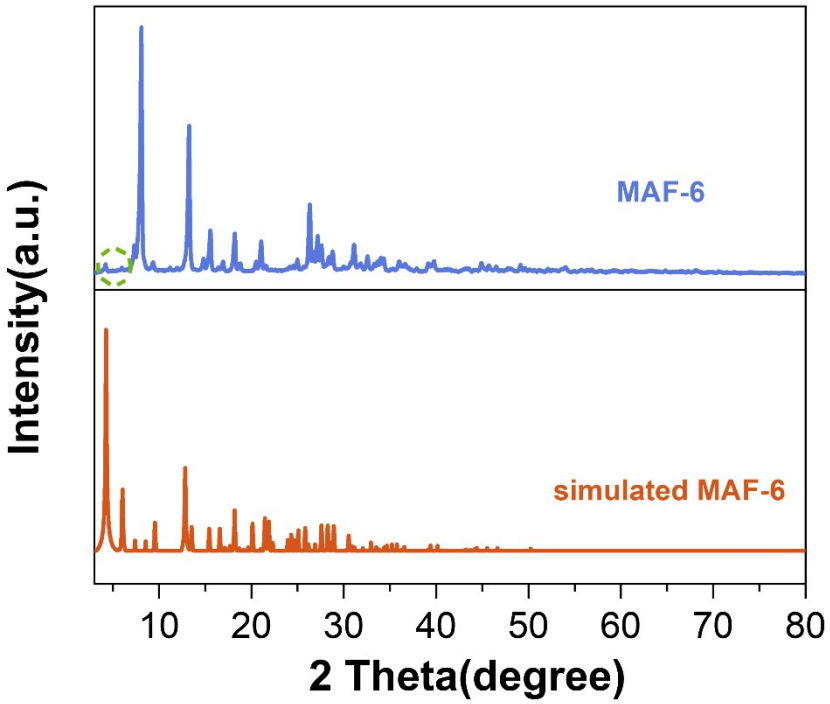

Fig. S1. XRD pattern of MAF-6.

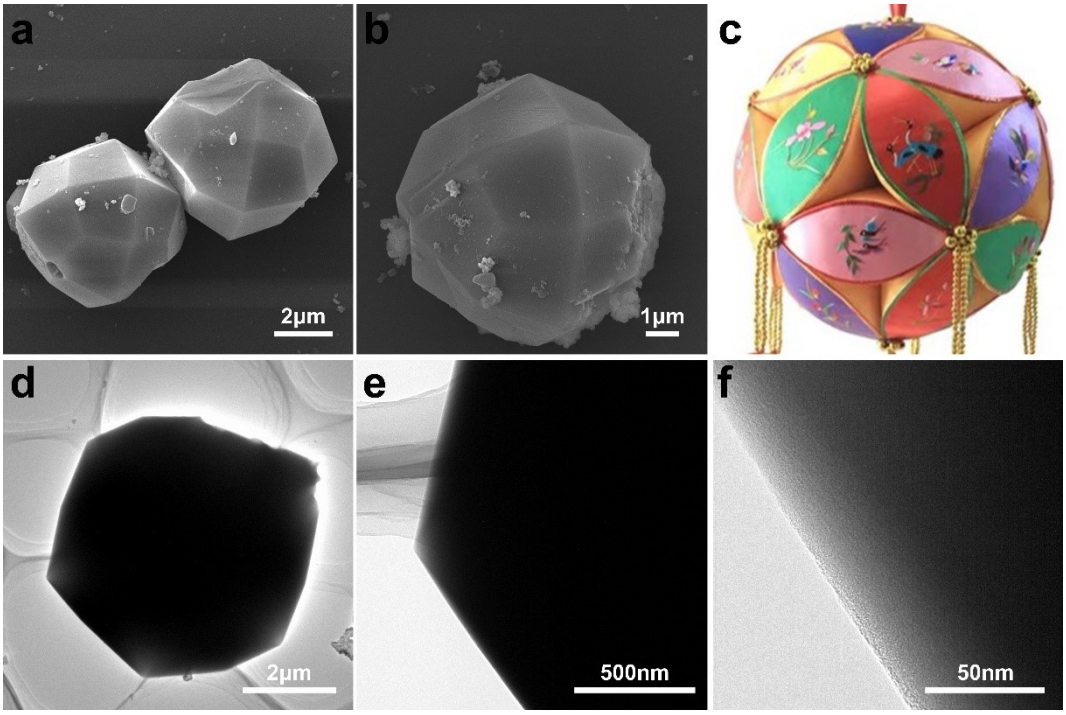

Fig. S2. SEM and TEM images of the MAF-6 samples. a, b) SEM images of MAF-6; c) The images of embroidered ball; d-f) TEM images of MAF-6.

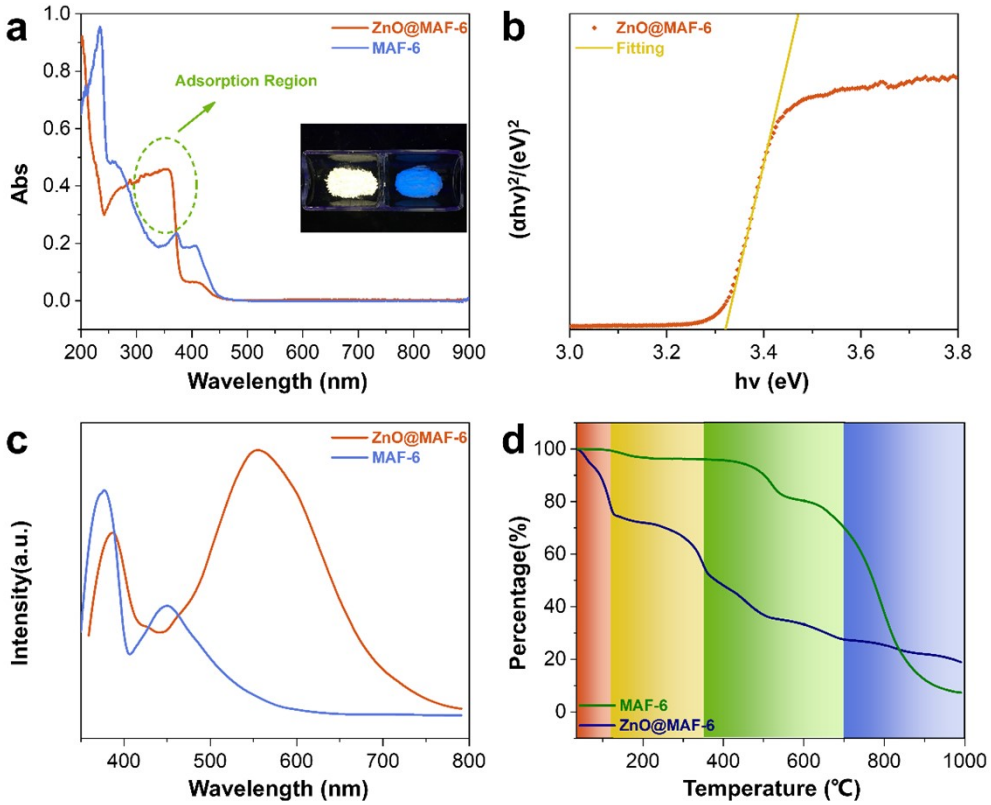

Fig. S3. a) Solid state UV-Vis absorption spectra of MAF-6 and ZnO@MAF-6, the illustration is the photo of two samples in the 365 nm UV lamp dark box (left: ZnO@MAF-6; right: MAF-6); b) Optical band gap fitting diagram of ZnO@MAF-6; c) Photoluminescence spectra of MAF-6 and ZnO@MAF-6; d) Thermogravimetric spectra of MAF-6 and ZnO@MAF-6.

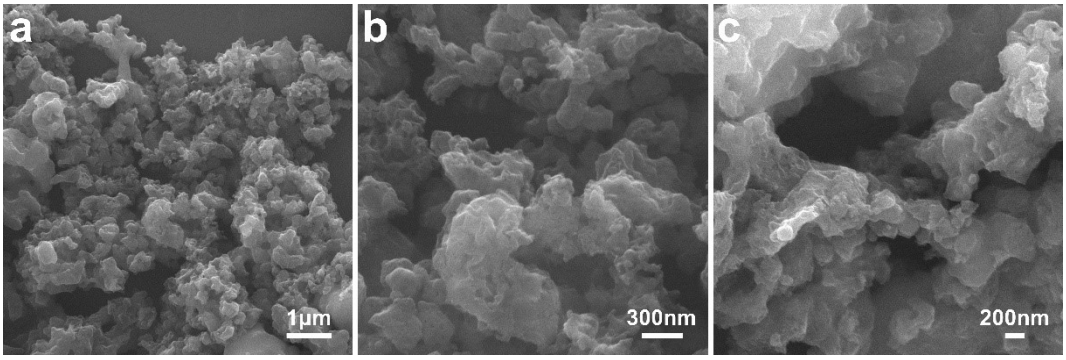

Fig. S4. SEM images of the N-DC samples.

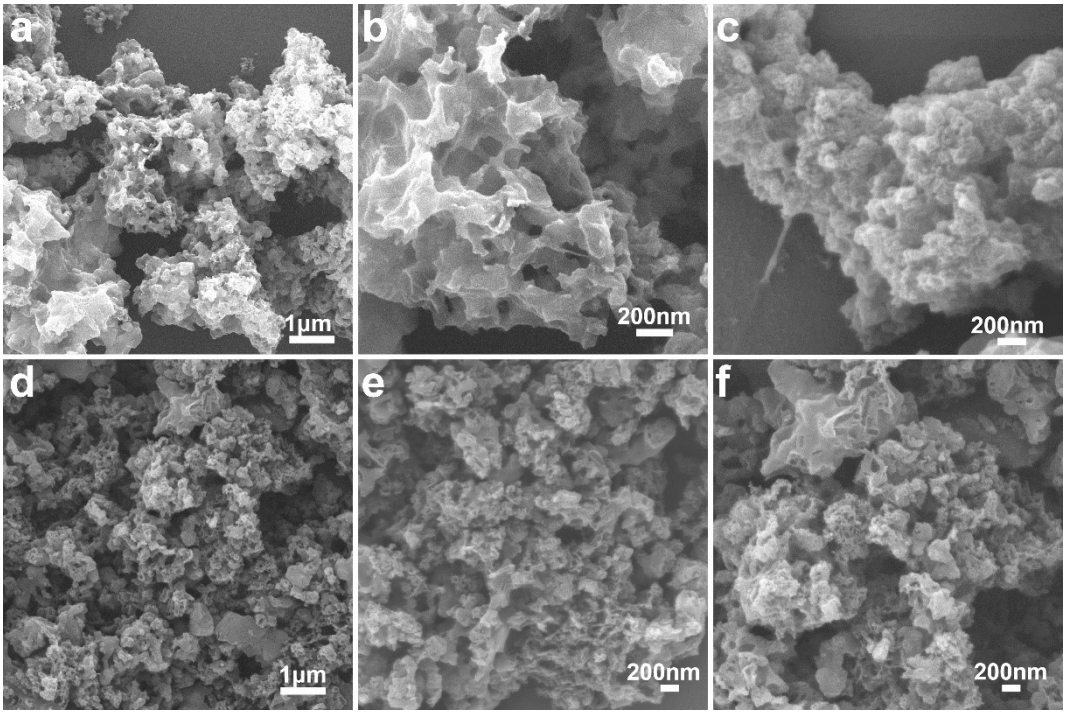

Fig. S5. a-c) SEM images of the DC samples; d-f) SEM images of the S-DC samples.

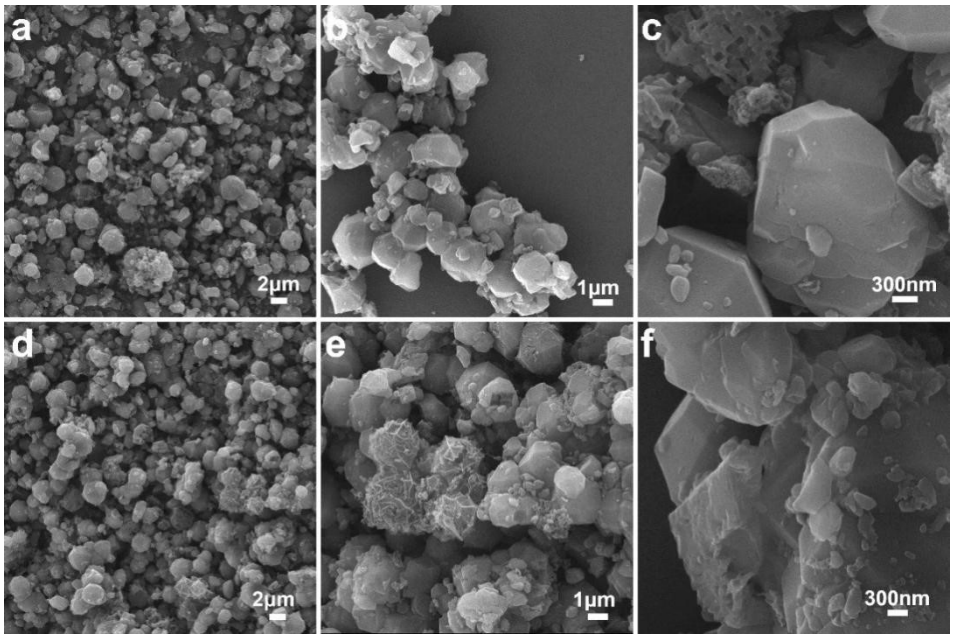

Fig. S6. a-c) SEM images of the N-C samples; d-f) SEM images of the N/S-C samples.

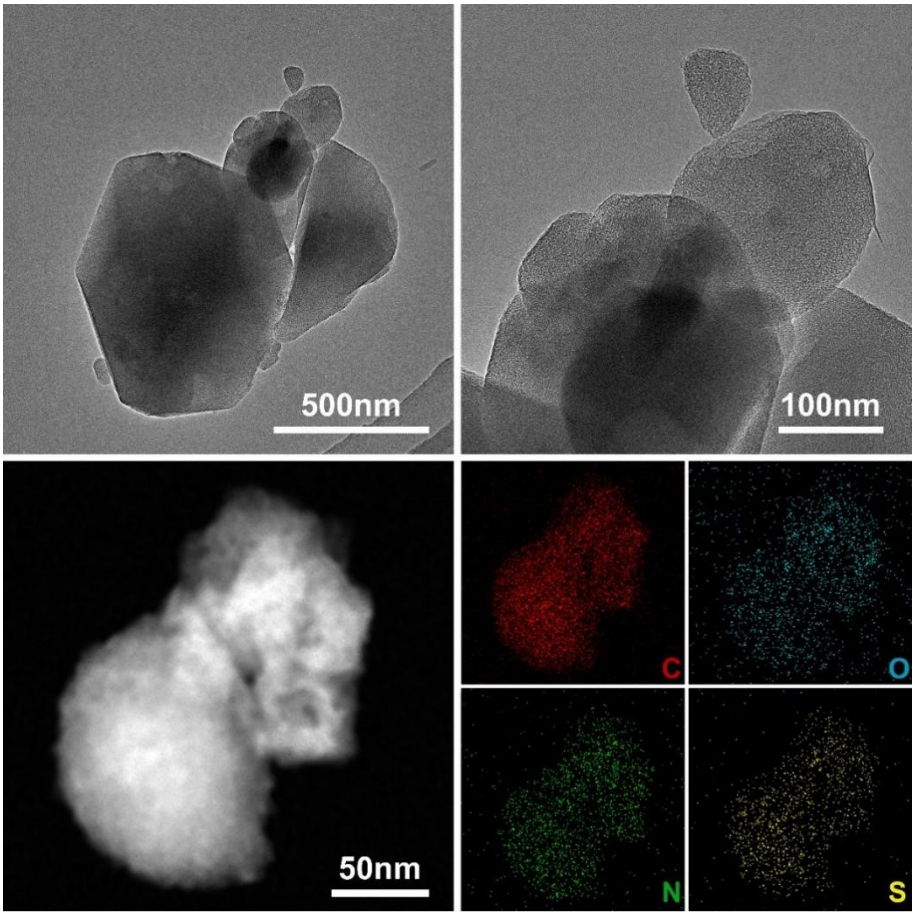

Fig. S7. TEM, HRTEM and mapping images of N/S-C.

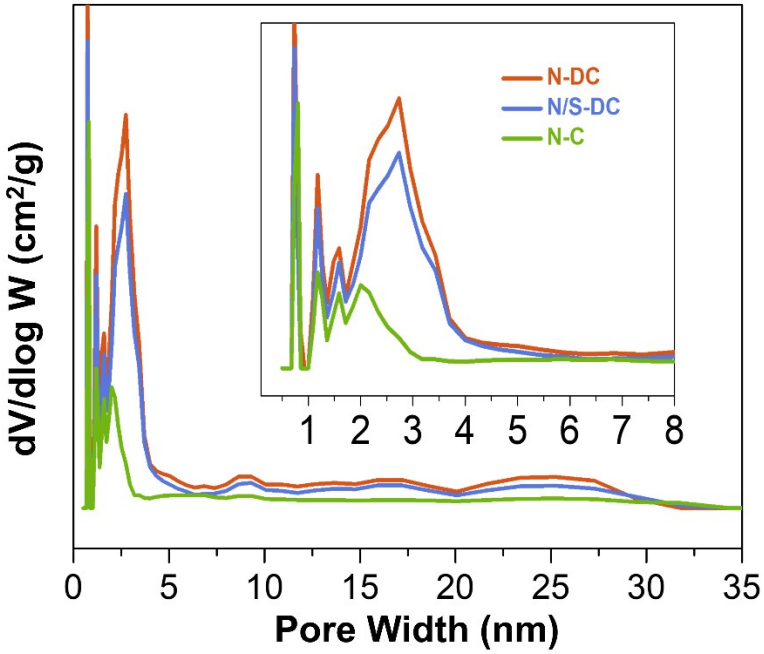

Fig. S8. The Pore size distribution of N-DC, N/S-DC and N-C by DFT model.

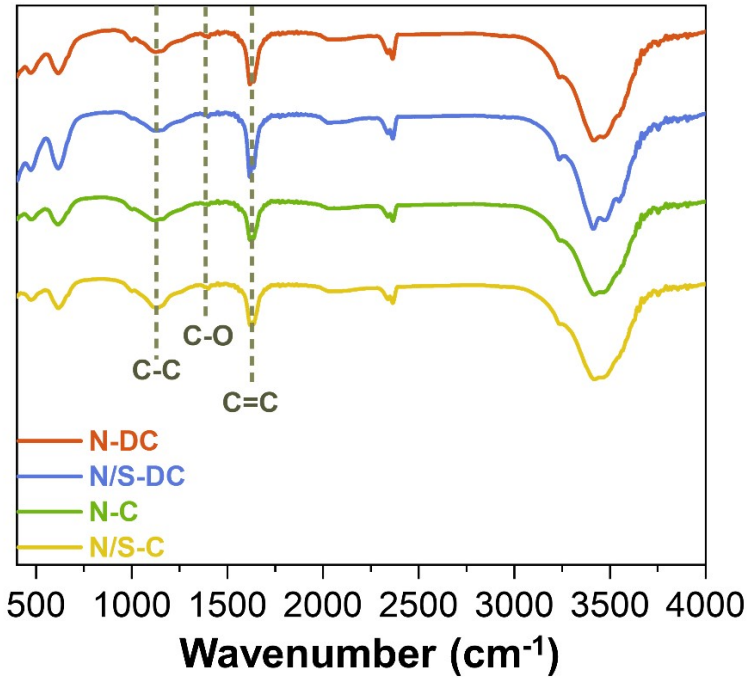

Fig. S9. FT-IR analysis of N-DC、N/S-DC、N-C and N/S-C.

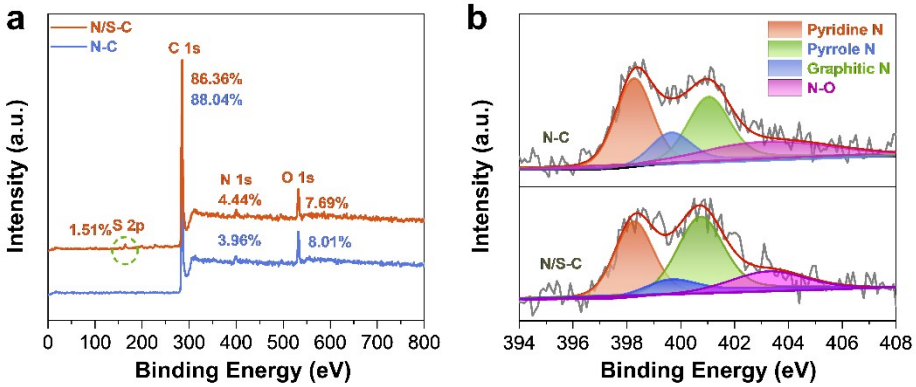

Fig. S10. a) XPS survey scan of N-C and N/S-C; b) The N 1s high-resolution XPS spectra of N-C and N/S-C.

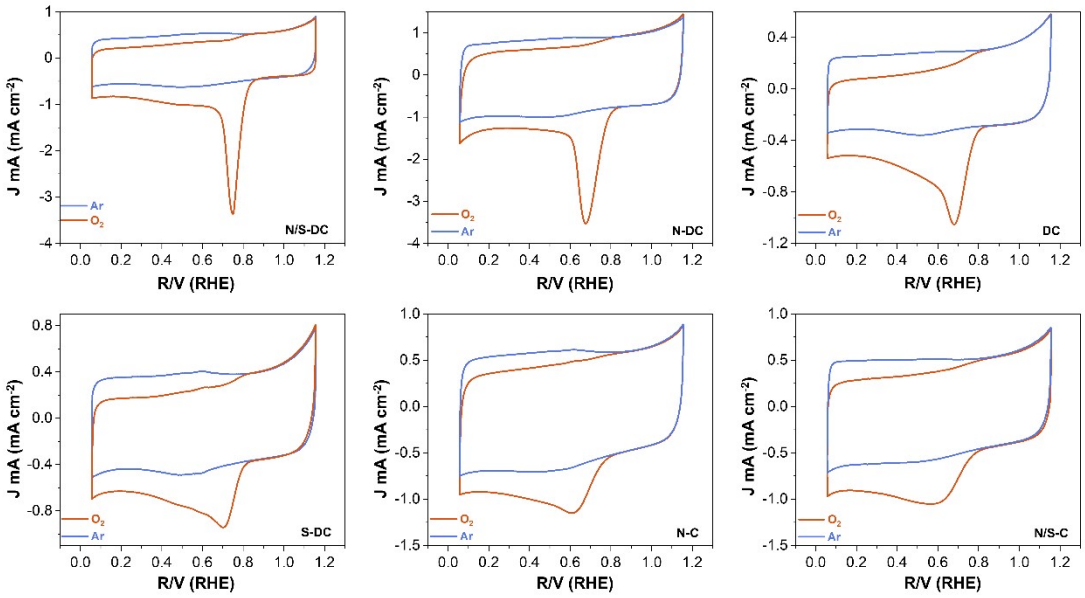

Fig. S11. CV of N/S-DC, N-DC, DC, S-DC, N-C and N/S-C in O_2-saturated and Ar-saturated 0.1 M $HClO_4$ solution.

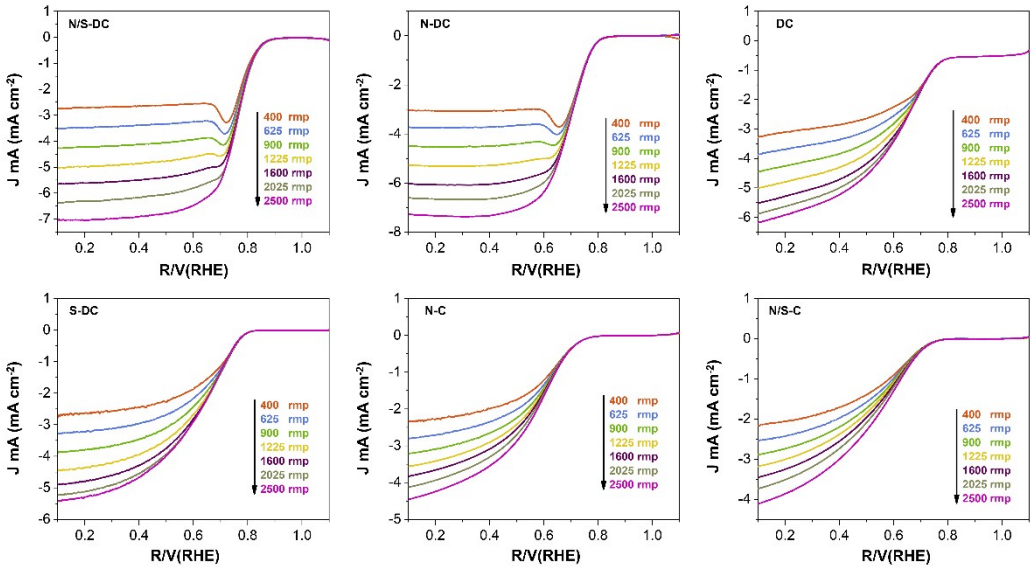

Fig. S12. LSV curves at various rotating speeds of N/S-DC, N-DC, DC, S-DC, N-C and N/S-C in 0.1 M $HClO_4$ solution.

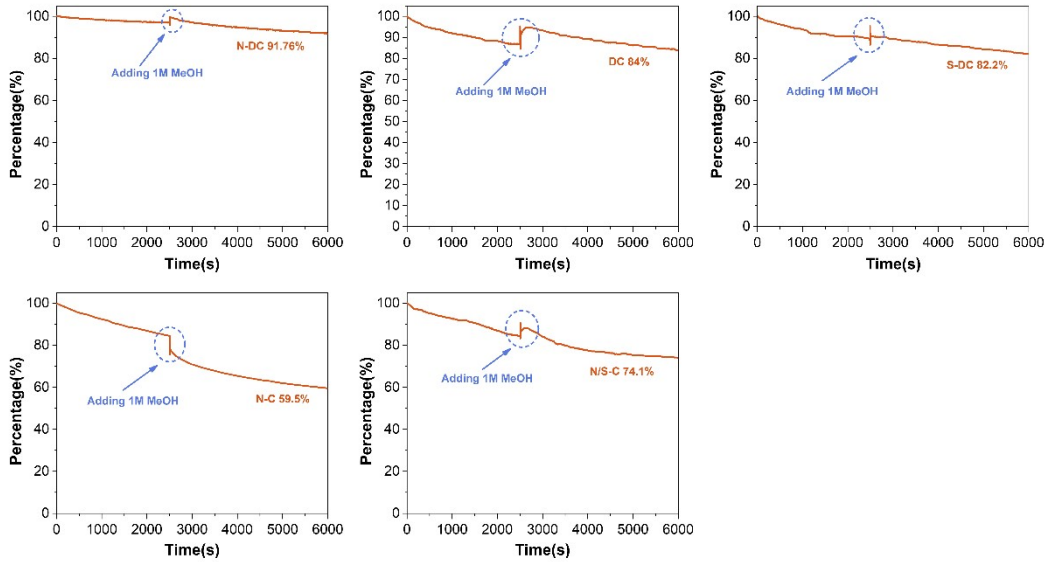

Fig. S13. *I-T* curves of S, DC, S-DC, N-C and N/S-C by adding 1 M MeOH at 2500 s in 0.1 M $HClO_4$ solution.

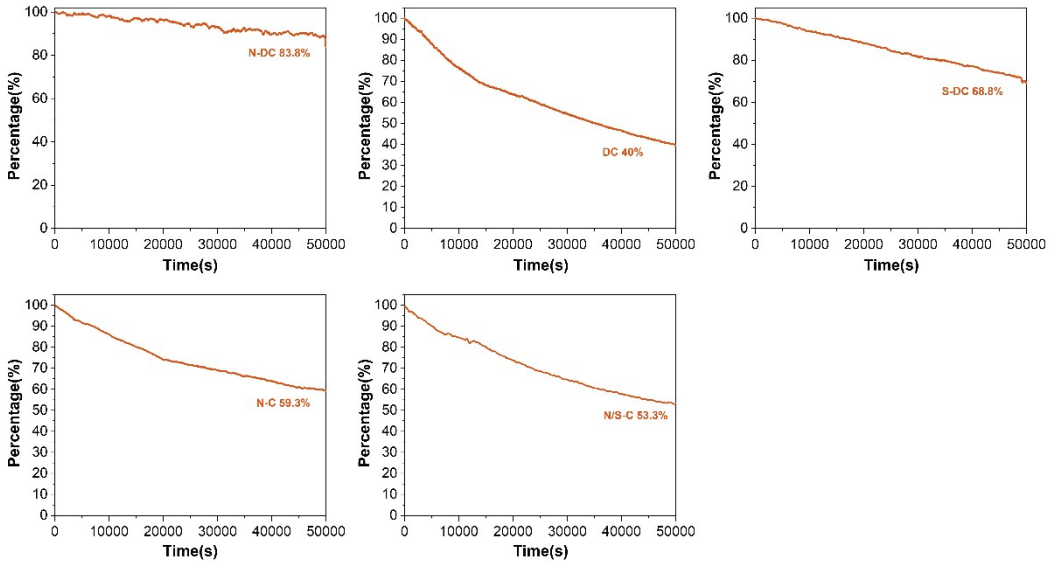

Fig. S14. The stability testing of N-DC, DC, S-DC, N-C and N/S-C in 0.1 M $HClO_4$.

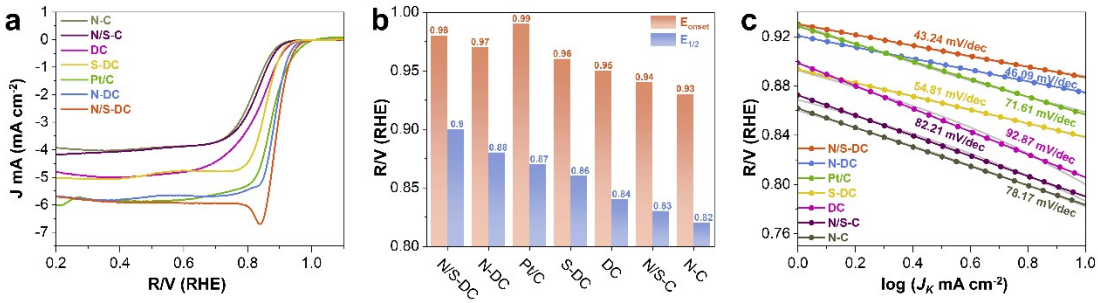

Fig. S15. a) ORR polarization plots for different catalysts and 20% Pt/C in 0.1 M KOH solution under O_2 saturation; b) E_{onset} and $E_{1/2}$ of different catalysts; c) Tafel slopes of different catalysts and 20% Pt/C.

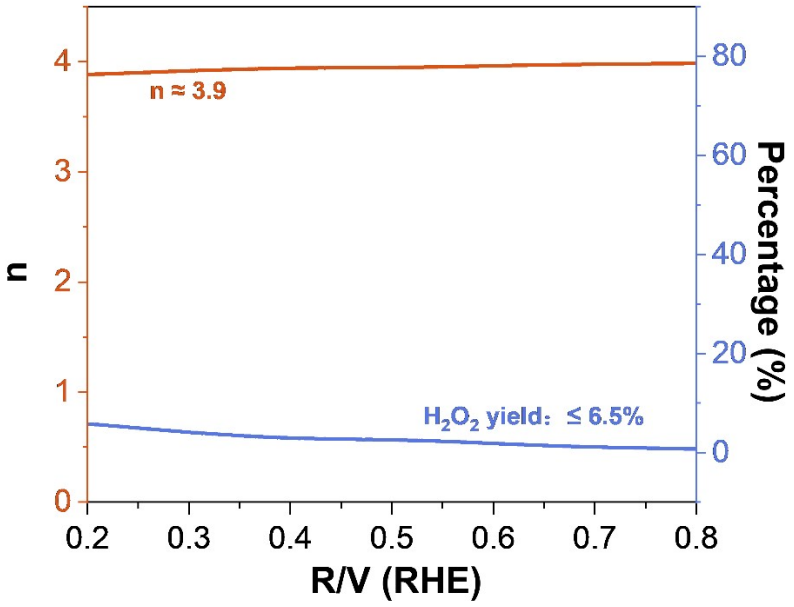

Fig. S16. Percentage of peroxide and electron transfer number of N/S-DC in 0.1 M KOH solution.

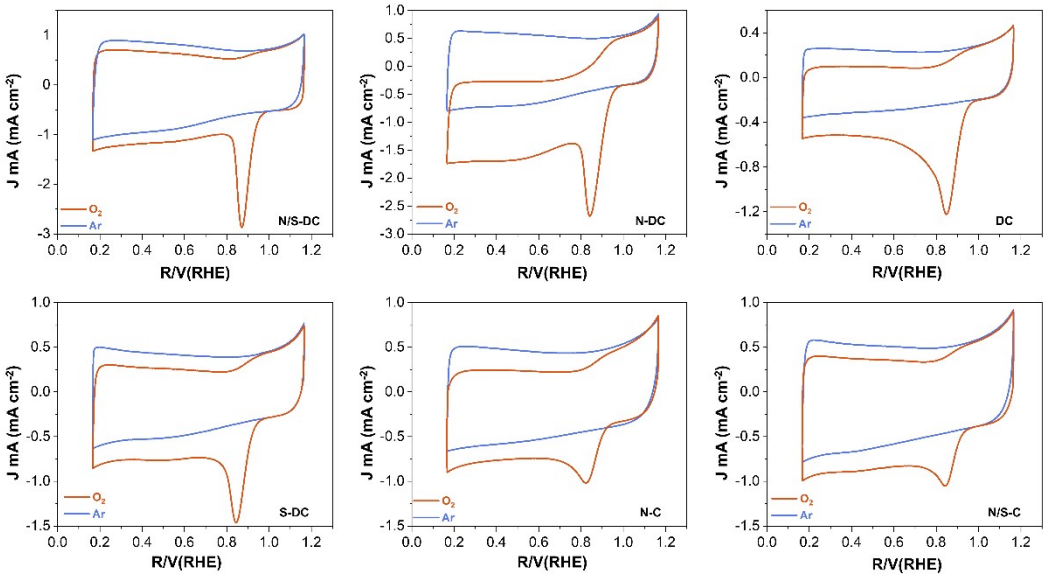

Fig. S17. CV of N/S-DC, N-DC, DC, S-DC, N-C and N/S-C in O_2-saturated and Ar-saturated 0.1 M KOH solution.

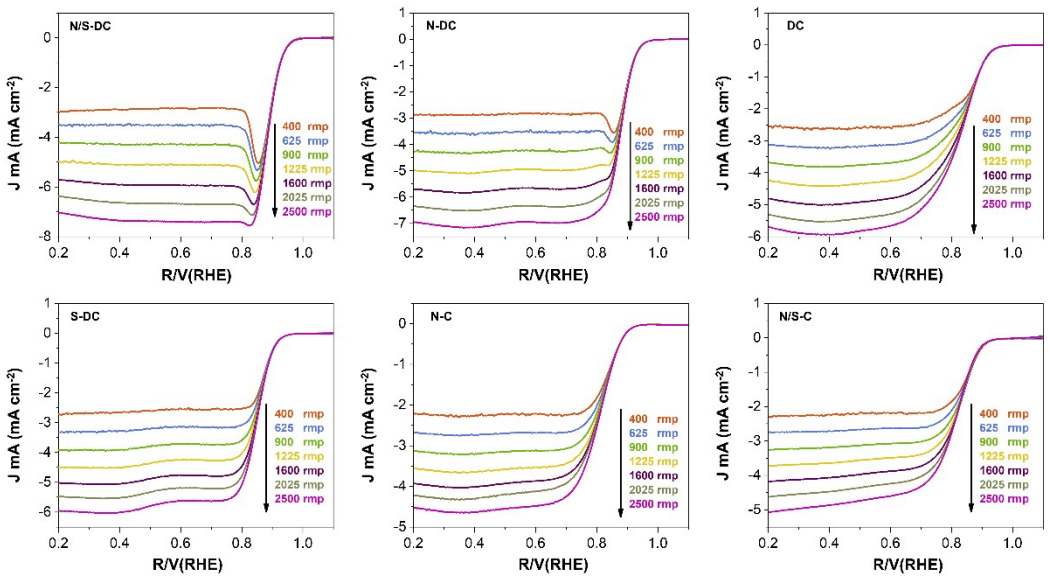

Fig. S18. LSV curves at various rotating speeds of N/S-DC, N-DC, DC, S-DC, N-C and N/S-C in 0.1 M KOH solution.

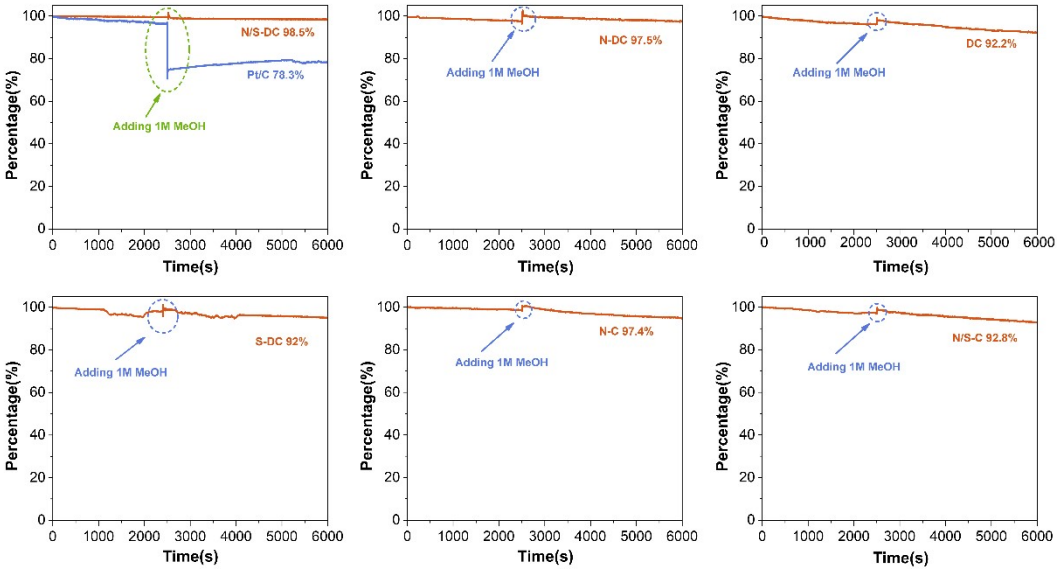

Fig. S19. *I-T* curves of N/S-DC, 20% Pt/C, N-DC, DC, S-DC, N-C and N/S-C by adding 1 M MeOH at 2500 s in 0.1 M KOH solution.

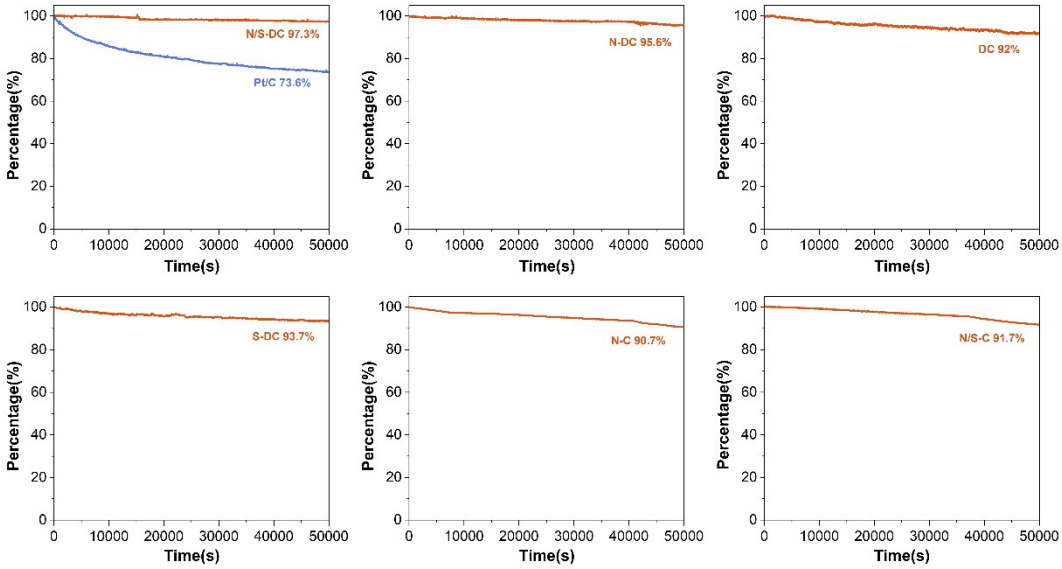

Fig. S20. The stability testing of N/S-DC, 20% Pt/C, N-DC, DC, S-DC, N-C and N/S-C in 0.1 M KOH.

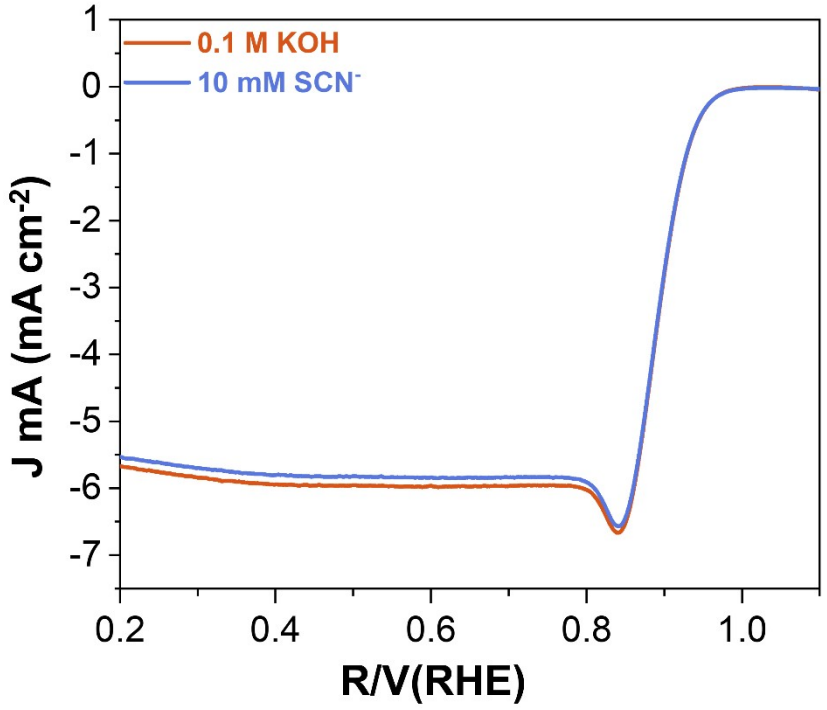

Fig. S21. LSV polarization curve of SCN^- interference test in N/S-DC sample in 0.1 M KOH solution.

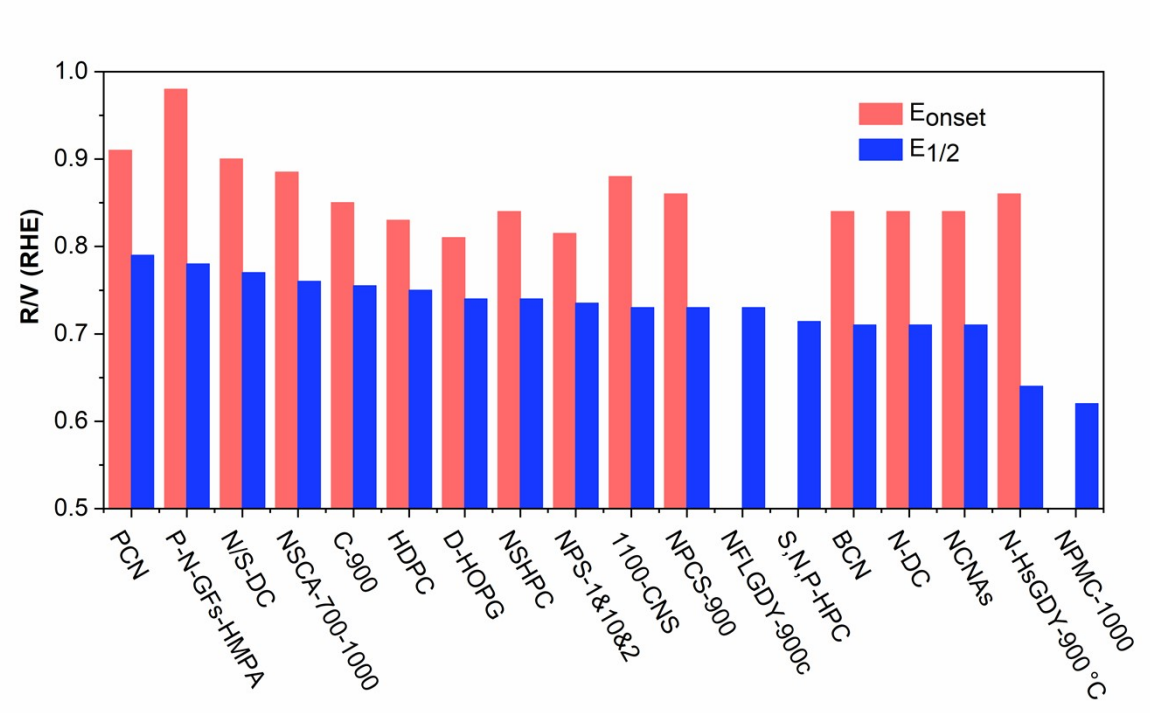

Fig.S22 Comparison of the E_{onset} and $E_{1/2}$ of some metal-free catalysts with excellent catalytic performance in acidic media, in which the specific value was summaried in Table S2 [2-20].

Table S1. Inductively Coupled Plasma (ICP-MS) test of N/S-DC.

Element	wt%
Zn	0.06338
Fe	0.045362
Co	0.004463
Ni	0.003933
Pt	0.002867

Table S2. Comparison of the ORR performance of some metal-free catalysts with excellent performance in acidic and alkaline media.

Catalyst	E_{Onset} (V vs. RHE) (acidic)	$E_{1/2}$ (V vs. RHE) (acidic)	E_{Onset} (V vs. RHE) (alkaline)	$E_{1/2}$ (V vs. RHE) (alkaline)	Ref.
N/S-DC	0.90	0.77	0.98	0.90	This work
N-DC	0.84	0.71	0.97	0.88	This work
HDPC	0.83	0.75	1.0	0.90	[2]
NDC-1000	-	-	0.96	0.86	[3]
NPS-G-2	-	-	-	0.857	[4]
ND-GLC	-	-	-	0.875	[5]
NSCA-700-1000	0.885	0.76	-	0.85	[6]
1100-CNS	0.88	0.73	0.99	0.85	[7]
NPMC-1000	-	0.62	0.94	0.85	[8]
NFLGDY-900c	-	0.73	-	0.87	[9]
D-HOPG	0.81	0.74	-	-	[10]
BCN	0.84	0.71	0.94	0.82	[11]
P–N-GFs-HMPA	0.98	0.78	1.04	0.84	[12]
PCN	0.91	0.79	-	-	[13]
S,N,P-HPC	-	0.714	-	0.881	[14]
NPS-1&10&2	0.815	0.735	0.948	0.862	[15]
NPCS-900	0.86	0.73	0.99	0.87	[16]
NCNAs	0.84	0.71	1.01	0.91	[17]
NSHPC	0.84	0.74	1.04	0.89	[18]
C-900	0.85	0.755	1.030	0.916	[19]
N-HsGDY-900 °C	0.86	0.64	1.02	0.85	[20]

References

[1] C. T. He, L. Jiang, Z. M. Ye, R. Krishna, Z. S. Zhong, P. Q. Liao, J. Xu, J. Ouyang, J. P. Zhang and X. M. Chen, Exceptional hydrophobicity of a large-pore metal–organic zeolite, *J. Am. Chem. Soc*., 2015, **137**, 7217-7223.

[2] Q. Wu, Y. Jia, Q. Liu, X. Mao, Q. Guo, X. Yan, J. Zhao, F. Liu, A. Du, and X. Yao, Ultra-dense carbon defects as highly active sites for oxygen reduction catalysis, *Chem*, 2022, **8**, 2715-2733.

[3] Q. Lai, J. Zheng, Z. Tang, D. Bi, J. Zhao and Y. Liang, Optimal configuration of N-doped carbon defects in 2D turbostratic carbon nanomesh for advanced oxygen reduction electrocatalysis, *Angew. Chem. Int. Ed.*, 2020, **59**, 11999-12006.

[4] X. Zheng, J. Wu, X. Cao, J. Abbott, C. Jin, H. Wang, P. Strasser, R. Yang, X. Chen and G. Wu, N-, P-, and S-doped graphene-like carbon catalysts derived from onium salts with enhanced oxygen chemisorption for Zn-air battery cathodes, *Applied Catalysis B: Environmental*, 2019, **241**, 442-451.

[5] J. Zhang, Y. Sun, J. Zhu, Z. Kou, P. Hu, L. Liu, S. Li, S. Mu and Y. Huang, Defect and pyridinic nitrogen engineering of carbon-based metal-free nanomaterial toward oxygen reduction, *Nano Energy*, 2018, **52**, 307-314.

[6] D. Li, Y. Jia, G. Chang, J. Chen, H. Liu, J. Wang, Y. Hu, Y. Xia, D. Yang and X. Yao, A defect-driven metal-free electrocatalyst for oxygen reduction in acidic electrolyte, *Chem*, 2018, **4**, 2345-2356.

[7] Z. Pei, H. Li, Y. Huang, Q. Xue, Y. Huang, M. Zhu, Z. Wang and C. Zhi, Texturing in situ: N,S-enriched hierarchically porous carbon as a highly active reversible oxygen electrocatalyst, *Energy Environ. Sci.*, 2017, **10**, 742-749.

[8] J. Zhang, Z. Zhao, Z. Xia and L. Dai, A metal-free bifunctional electrocatalyst for oxygen reduction and oxygen evolution reactions, Nat. *Nanotechnol.*, 2015, **10**, 444-452.

[9] Y. S. Zhao, J. W. Wan, H. Y. Yao, L. J. Zhang, K. F. Lin, L. Wang, N. L. Yang, D. B. Liu, L. Song, J. Zhu, L. Gu, L. Liu, H. J. Zhao, Y. L. Li and D. Wang, Few-layer graphdiyne doped with sp-hybridized nitrogen atoms at acetylenic sites for oxygen reduction electrocatalysis, *Nat. Chem.*, 2018, **10**, 924-931.

[10] Y. Jia, L. Z. Zhang, L. Z. Zhuang, H. L. Liu, X. C. Yan, X. Wang, J. D. Liu, J. C. Wang, Y. R. Zheng, Z. H. Xiao, E. Taran, J. Chen, D. J. Yang, Z. H. Zhu, S. Y. Wang, L. M. Dai and X. D. Yao, Identification of active sites for acidic oxygen reduction on carbon catalysts with and without nitrogen doping, *Nat. Catal.*, 2019, **2**, 688-695.

[11] J. M. Wang, J. Hao, D. Liu, S. Qin, D. Portehault, Y. W. Li, Y. Chen and W. W. Lei, Porous boron carbon nitride nanosheets as efficient metal-free catalysts for the oxygen reduction reaction in both alkaline and acidic solutions, *ACS Energy Lett*., 2017, **2**, 306-312.

[12] C. L. Li, Z. Y. Chen, A. G. Kong, Y. Y. Ni, F. T. Kong and Y. K. Shan, High-rate oxygen electroreduction over metal-free graphene foams embedding P-N coupled moieties in acidic media, *J. Mater. Chem. A*, 2018, **6**, 4145-4151.

[13] T. Najam, S. S. A. Shah, W. Ding, J. X. Jiang, L. Jia, W. Yao, L. Li and Z. D. Wei, An efficient anti-poisoning catalyst against SOx, NOx, and POx: P, N-doped carbon for oxygen reduction in acidic media, *Angew. Chem. Int. Ed.*, 2018, **57**, 15101-15106.

[14] Y. X. Zan, Z. P. Zhang, M. L. Dou and F. Wang, Enhancement mechanism of sulfur dopants on the catalytic activity of N and P co-doped three-dimensional hierarchically porous carbon as a metal-free oxygen reduction electrocatalyst, *Catal. Sci. Technol*., 2019, **9**, 5906-5914.

[15] Y. D. Long, F. H. Ye, L. Shi, X. N. Lin, R. Paul, D. Liu and C. G. Hu, N, P, and S tri-doped holey carbon as an efficient electrocatalyst for oxygen reduction in whole pH range for fuel cell and zinc-air batteries, *Carbon*, 2021, **179**, 365-376.

[16] G. Y. Ren, S. Q. Chen, J. X. Zhang, N. J. Zhang, C. L. Jiao, H. F. Qiu, C. X. Liu and H. L. Wang, N-doped porous carbon spheres as metal-free electrocatalyst for oxygen reduction reaction, *J. Mater. Chem. A*, 2021, **9**, 5751-5758.

[17] G. Y. Ren, Q. S. Chen, J. G. Zheng, B. Huang and Y. Qian, N-doped carbon nanofibers aerogels derived from aramid as efficient electrocatalysts for oxygen reduction reaction in alkaline and acidic media, *J. Electroanal. Chem*., 2018, **829**, 177-183.

[18] R. R. Li, F. Liu, Y. H. Zhang, M. M. Guo and D. Liu, Nitrogen, sulfur Co-doped hierarchically porous carbon as a metal-free electrocatalyst for oxygen reduction and carbon dioxide reduction reaction, *ACS Appl. Mater. Interfaces*, 2020, **12**, 44578-44587.

[19] Q. Wu, Q. Liu, Y. Zhou, Y. Sun, J. Zhao, Y. Liu, F. Liu, M. Nie, F. Ning, N. Yang, X. Jiang, X. Zhou, J. Zhong and Z. Kang, Carbon defect-induced reversible carbon-oxygen interfaces for efficient oxygen reduction, *ACS Appl. Mater. Interfaces*, 2018, **10**, 39735-39744.

[20] Q. Lv, W. Si, J. He, L. Sun, C. Zhang, N. Wang, Z. Yang, X. Li, X. Wang, W. Deng, Y. Long, C. Huang and Y. Li, selectively nitrogen-doped carbon materials as superior metal-free catalysts for oxygen reduction, *Nat Commun.*, 2018, **9**, 3376.